

We are IntechOpen, the world's leading publisher of Open Access books Built by scientists, for scientists

6,900

Open access books available

186,000

International authors and editors

200M

Downloads

Our authors are among the

154

Countries delivered to

TOP 1%

most cited scientists

12.2%

Contributors from top 500 universities



WEB OF SCIENCE™

Selection of our books indexed in the Book Citation Index
in Web of Science™ Core Collection (BKCI)

Interested in publishing with us?
Contact book.department@intechopen.com

Numbers displayed above are based on latest data collected.
For more information visit www.intechopen.com



Studying a LW-VCSEL-Based Resonant Cavity Enhanced Photodetector and Its Application in Microwave Photonics Circuits

Mikhail E. Belkin, Leonid I. Zhukov, Dmitriy A. Fofanov, Mikhail G. Vasil'ev and Alexander S. Sigov

Abstract

A detailed comparative experimental study was carried out to pursue advanced performances corresponding to the key parameters of two photodetectors based on vertical cavity surface emitting laser (VCSEL) operating in free-running or optically injection locked mode, as well as an inherent pin-photodetector. During the preliminary study, the key static and dynamic parameters were quantitatively determined and the optimal operating modes were derived for the both versions of VCSEL-based photodetectors as separate microwave-photonics circuit elements. Based on them, a final experiment was conducted to evaluate the processing quality, when one of the versions of VCSEL-based photodetectors or a inherent pin-photodetector is implemented as an optical-to-electrical converter for a typical microwave-photonics circuit that processes 120-Mbps 16-position quadrature amplitude modulated signal on the radio frequency carrier of 1–6 GHz. As a result, it was confirmed that better processing quality, i.e. Error Vector Magnitude value of less than 4%, could be obtained by using the free-running VCSEL-based photodetector version.

Keywords: resonant cavity enhanced photodetector, long-wavelength vertical cavity surface emitting laser, optically injection locking, microwave photonics, optoelectronic processing

1. Introduction

As well known, a pin-structured semiconductor photodetector (PD) is the most important active element of world-spread fiber-optics communication systems (FOCS) [1], where it performs the functions of an effective optical-electric converter (OEC) in the receiver unit located at the far end of a telecom link. Additionally, in the last decade, this device has found wide application in the intensively developing radio electronic systems (RES) for civil and military purposes based on microwave photonics (MWP) technology [2, 3]. In these systems, the MWP circuitry also contains two more requisite units that carry out electrical-optic conversion (EOC) and processing of radio-frequency (RF) signals in the optical domain [4]. Therein, the EOC operation is realized either by direct

modulation of a semiconductor laser's injection current or by external modulation of an optical modulator pumped by a laser source power. After optical processing such as transmission, amplifying, filtering, time delay, etc., an OEC operation must be performed, for the implementation of which a pin-photodetector is used. Thus, unlike traditional FOCSs, both a laser and a photodetector must be present in a common MWP circuit, which paves the way for its simplifying and, therefore, reducing the cost of the device by combining EOC and OEC functions.

The study of the structures and constructions of modern photodiode and widespread edge emitting laser showed that the former cannot operate in the lasing mode, since there is no amplification layer and optical resonators that provide positive feedback. In addition, the latter is not suitable for operation in a photodetector mode, in principle, since it has a completely different design and even a very small reverse biasing leads to its failure. However, there is a semiconductor laser of a different design: a vertical cavity surface-emitting laser (VCSEL) with an epitaxial structure similar to a photodetector [5, 6], and its long-wavelength version (LW-VCSEL) has a great potential for the application in modern and prospective FOCSs [7] as well as in MWP circuits [8].

In general, a resonant cavity enhanced (RCE) PD based on a pin-photodiode or a Schottky-barrier photodiode is a long-time known optoelectronic device that overcomes the fundamental drawback of an inherent photodetector associated with a compromise between bandwidth and sensitivity [9, 10]. Its design with an active depletion region between two multilayer mirrors of a Fabry-Perot resonator is similar to a VCSEL. Modern development follows the path of researching and fabricating both individual RCE-PD chips in the short-wavelength or long-wavelength telecom spectral range [11, 12], as well as monolithically integrated chips containing on one substrate an optoelectronic pair based on a VCSEL and a RCE-PD [13]. So that, during a literature search, a publication was found [14] reporting the results of an experimental study of RCE photodiode based on a short-wavelength VCSEL with a quantum-well active region operating in the photovoltaic mode or in reverse bias mode. This technological study was carried out in order to determine the conditions for ensuring the maximum quantum efficiency of the OEC, which was regulated by sequentially etching the layers of the upper mirror, as well as the conditions for ensuring the maximum width of the frequency characteristic at the output. The latter was controlled by adjusting the diameter of the active layer.

The motivation for our recent investigation in this direction [15] was to measure the static and dynamic characteristics of the particular LW-VCSEL sample without any structural changes. For this goal, we simply reversed the DC bias polarity to assess the efficiency of its use as part of an optoelectronic coupler based on two identical LW-VCSEL chips, one of which worked as a laser source, and the other as a photodetector. An additional goal was to demonstrate the effective operation of a LW-VCSEL-based RCE photodetector (VCSEL-PD) in an economical photoreceiver for the currently widespread digital FOCS with dense wavelength division multiplexing (DWDM), due to the absence of a spectral demultiplexer needed for a standard DWDM FOCS. Leveraging this concept, two other applications combining LW-VCSEL in the laser and photodetector modes have recently been investigated including the uses in a high-speed optoelectronic switch device for integrated photonics-based optical beamforming network [16] and in cost-efficient optoelectronic frequency-converting transceiver for a base station of 5G cellular communication network [17].

To date, there is one more version of LW-VCSEL-based photodetector [18, 19], where a new concept using such an effective laser technique, especially for low-power VCSEL, as optical injection locking (OIL) [20, 21], was proposed and preliminary investigated. From the operational point of view, an obvious advantage

of this approach compared to our one is the possibility of full-duplex operation in a combined EOC/OEC without switching the polarity of the power supply. In the cited papers, an integrated consideration is used that addresses the effect of expanding the bandwidth of an OIL VCSEL-based photodetector (OIL-VCSEL-PD) and experimental study of the signal quality (bit error rate) in a FOCS, when digital signals at a speed of 12 Gbps are transmitted. However, the key parameters of the OIL-VCSEL-PD itself, such as responsivity, the level of introduced noise, etc., have not been studied at all.

As a result, in present scientific publications there is no clear answer to the question of selecting the optimal photodetector for the application in microwave- photonics circuits. Eliminating it, this Chapter addresses a comparative experimental study reviewing the known, updated, and newer results to pursue advanced performances corresponding to the key OEC parameters of an inherent pin-photodetector as well as the two VCSEL-based photodetectors in free-running or OIL mode and their applications in the last generation of key MWP circuits for prospective photonics and radio-electronics systems. In particular, pursuing the goal to discovery optimal operation regimes for the VCSEL-based RCE photodetector, Section 2 reviews key features of the C-band (1530–1565 nm) free-running LW-VCSEL as the object for investigation. In addition, Section 3 presents the updated and newer results of measuring static and dynamic characteristics for the LW-VCSEL-based RCE photodetector under study in the above-mentioned operating modes. The results of design and comparative experimental research using a typical MWP circuit that includes OEC based on an inherent pin-photodetector or two versions of VCSEL-based RCE photodetectors under study are demonstrated in Section 4. Finally, Section 5 concludes the Chapter.

2. The object for investigation

For today, several technologies yielding LW-VCSEL with acceptable performances have been developed. Among them, wafer-fused LW-VCSELs under research (**Figure 1**) employing strained InP/InAlGaAs quantum well (QWs) active region, tunnel junction (TJ) for carrier and optical confinement, and distributed Bragg reflectors (DBR), have also reached the industrial production stage and proven reliability [8]. A particular preference of these LW-VCSELs is in covering the full ITU-T spectral range from O-band to U-band. Concerning MWP approach, an outstanding feature of LW-VCSELs is their compatibility with future large-scale silicon-based heterogeneous photonics integrated circuits [22], which should

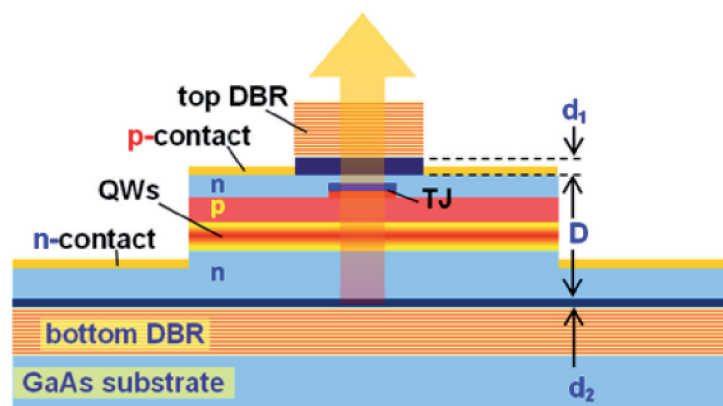


Figure 1.
Schematic of wafer-fused LW-VCSEL from beam express LLC, Switzerland.

provide many advantages when implementing MWP devices and techniques. The processing of the double-fused VCSEL wafer includes reactive ion etching in top DBR, selective chemical etching in the InAlGaAs/InP active cavity region, dielectric deposition, dry etching, and e-beam deposition of metals for contacts [8]. The much smaller size of the active region (D) in comparison with the edge emitting laser requires several times higher reflection coefficients of the upper and lower mirrors to generate lasing conditions, which is provided due to high-Q DBRs based on 30 or more intermittent layers of GaAs/AlGaAs. These mirrors are fused to top and bottom parts of an each active region before dicing [23].

Figure 2 shows a microscope view of a tiny piece of a laser wafer with formed electrical pads. As seen, the processed VCSEL wafer offers on-wafer testing possibility that decreases manufacturing cost as compared to edge emitting lasers. Moreover, a pattern of the full wafer-electroplated anode and cathode pads is designed in such a way to ensure the correct testing using a standard microwave probe of GS-type.

All further measurements will carry out on the Probe Station (PS) EP6 from Cascade Microtech. The workbench including thermo-electrical cooler for temperature controlling, coplanar RF probe (on the left), and fiber-optics probe (on the right) is shown in **Figure 3**.

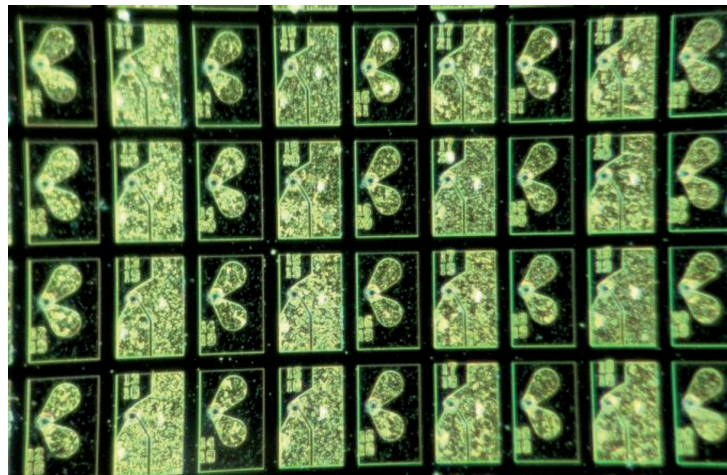


Figure 2.
A microscope view of the VCSEL wafer under study.



Figure 3.
The workbench for VCSEL chip's study.

Below we, using widespread techniques and procedures, will present typical static and needed for MWP characterization dynamic characteristics of the LW-VCSEL under test in free-running mode of its operation [8, 23] that will use further for examination of the same device in RCE photodetector modes. The testbed (see **Figure 4**) operates in three ranges: direct current (DC), RF, and C-band (1530–1565 nm) optical ones. Besides the VCSEL under test, it contains a set of accessories such as optical coupler (Opneti, CP10/90–1550), reference photodiode (Finisar, BPDV2150, 43-GHz bandwidth, 0.6-A/W responsivity), bias-T (Pasternack, PE1BT-1002, 40-GHz bandwidth) as well as corresponding DC power suppliers and measuring tools including optical spectrum analyzer (Yenista OSA20), optical power meter (EXFO PM-1100), RF vector network analyzer (Agilent E8363B).

Figure 5(a) depicts a PS-assisted light-current characteristic (LCC) of the LW-VCSEL under test emitting in the fundamental wavelength of 1560.95 nm at the room temperature. For the device under test, the threshold current is near 2.3 mA and a quasi-linear dependence of coupled optical power vs. current was observed up to 9 mA. To estimate the losses introduced by the optical probe, **Figure 5(b)** shows typical LCCs and a voltage–current characteristic of a C-band LW-VCSEL chip when registering its complete output power [8].

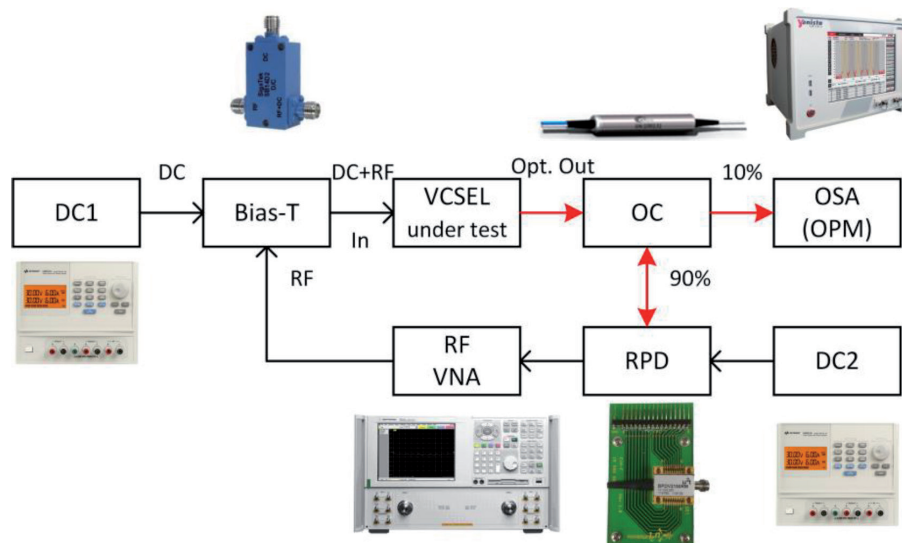


Figure 4. Common testbed for measuring static and dynamic characteristics of the object for investigation, where OC, RPD, OSA, OPM, and RF VNA stand for optical coupler, reference photodiode, optical spectrum analyzer, optical power meter, and RF vector network analyzer, respectively. (optical connections are painted in red, electrical connections – in black).

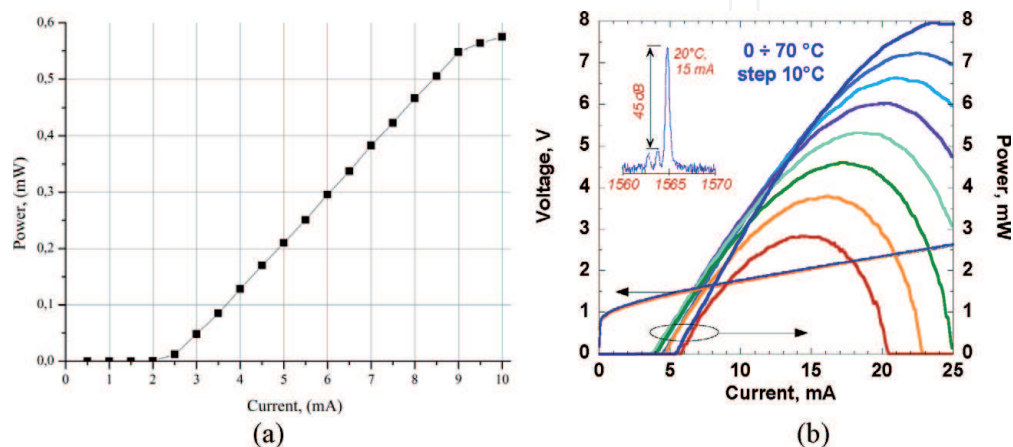


Figure 5. Light-current characteristics of the VCSEL chip under study: (a) Probe station-assisted; (b) Registering its complete output power [8].

Figure 6 shows an example of a PS-assisted spectral characteristic of the LW-VCSEL under test at the current of 6 mA, where a fundamental mode with the coupled power of -10 dBm at the wavelength of 1560.95 nm and a side-mode suppression ratio of 52 dB are observed.

In addition, **Figure 7** presents the spectral evolution of VCSEL emission with currents and temperature.

Figure 8 presents the small-signal transmission gain (TG) of an optoelectronic pair comprising the LW-VCSEL under test and RPD (see **Figure 4**). As one can see, at lower modulation frequencies the TG value is -30 dB and the -3 dB bandwidth of the LW-VCSEL under test is 3.7 GHz at 3-mA and more than 9 GHz at 10-mA bias current.

For the sake of completeness, we will end this section with a couple of examples characterizing the VCSEL under study in an optically injection locked mode.

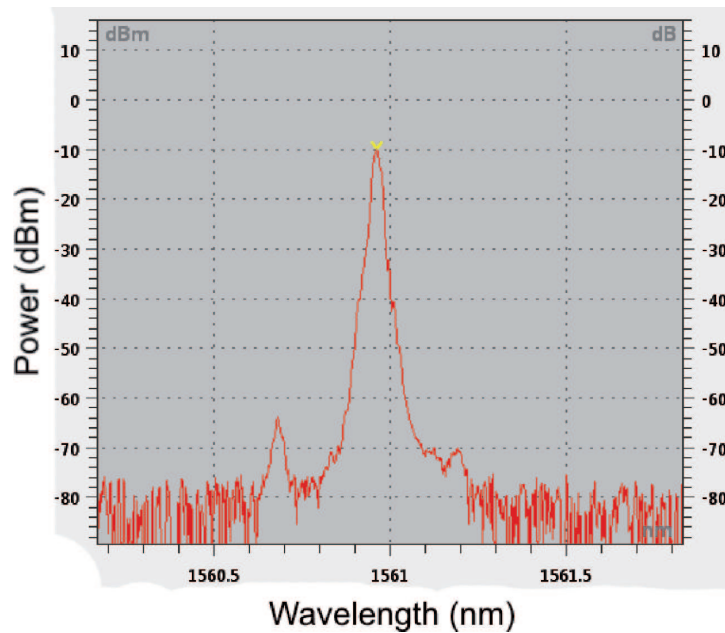


Figure 6.
Example of a spectral characteristic of the LW-VCSEL under test.

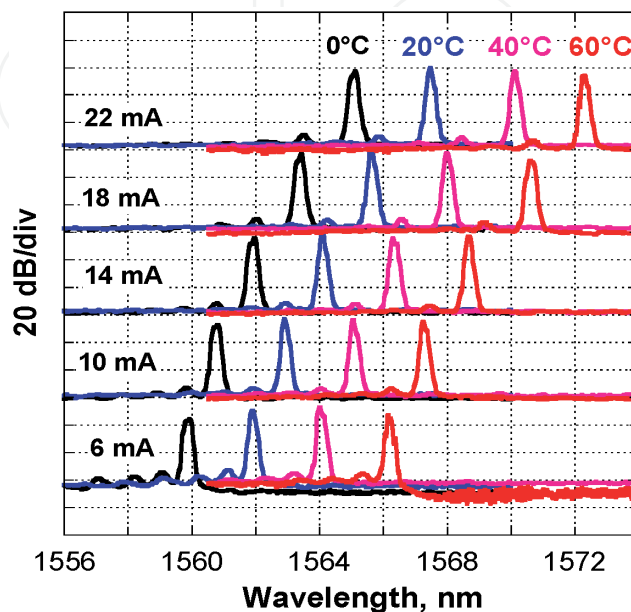


Figure 7.
Spectral evolution of the tested VCSEL emission with current and temperature.

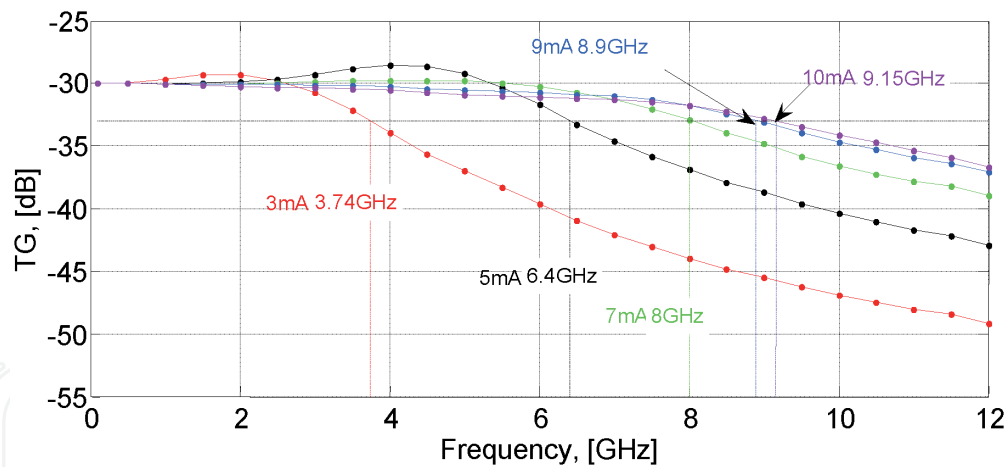


Figure 8.
 Small-signal transmission gain characteristics of the wafer-fused LW-VCSEL under test.

The measurements will be made using the testbed of **Figure 4** by replacing the block “VCSEL under test” with the block-diagram shown in **Figure 9**.

Figures 10 and **11** exemplify an optical spectrum and small-signal modulation characteristics of tested VCSEL in OIL mode.

The following outcomes for the further study can be drawn from this section.

- Comparison of LCC (**Figure 5(a)**) with the previously obtained measurement results for a similar characteristic of a VCSEL chip when registering a complete output power (see **Figure 5(b)**) allows us to assess the probe-assisted coupled factor at a level of 19% (losses of about 7.2 dB), which will be taken into account in further estimates.
- As follows from a comparison of the spectral characteristics for VCSEL in free-running (**Figure 6**) and OIL (**Figure 10**) modes, the effect of optical injection locking leads to a more than 10-dB increase in emitted power and to a pure single-frequency spectrum with almost 10-dB gain in side-mode suppression ratio.
- As it can be observed from **Figure 7**, combinations of temperature and driving current allow tuning the emission wavelength inside 12 nm with the separate current tuning of near 0.25 nm/mA and temperature tuning of near 0.1 nm/°C.
- As follows from a comparison of the small-signal modulation characteristics for VCSEL in free-running mode (**Figure 8**) at current of 8 mA and in OIL mode (**Figure 11**), effect of optical injection locking leads to more than 4-fold modulation bandwidth.

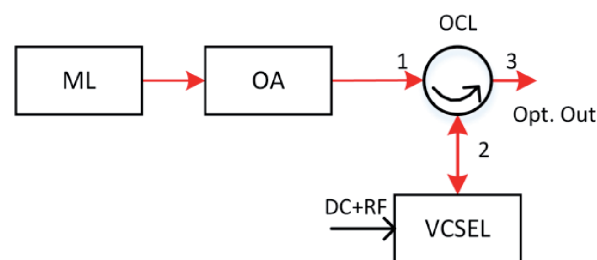


Figure 9.
 Conceptual block-diagram of OIL-VCSEL, where ML, OA, and OCL stand for master laser, optical amplifier, and optical circulator, respectively. (optical connections are painted in red, electrical connections – in black).

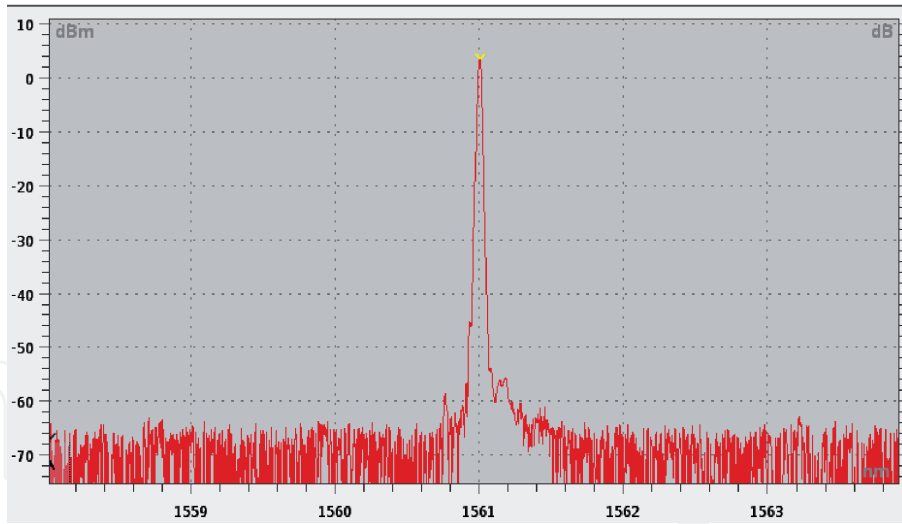


Figure 10.
Optical spectrum of the OIL-VCSEL under test.

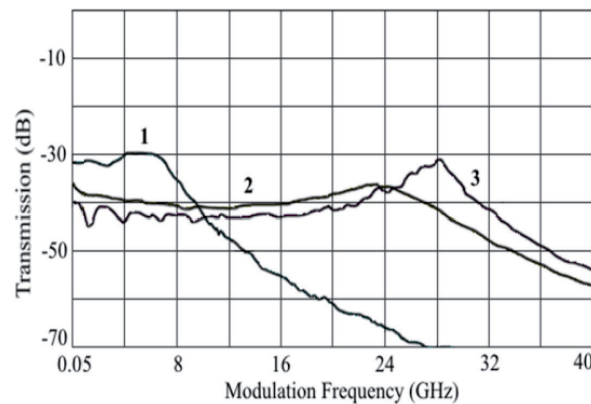


Figure 11.
Small-signal modulation characteristics of OIL-VCSEL under test in free-running mode (1), and in OIL mode when the power of the ML is 5 dBm (2) or 8 dBm (3).

3. VCSEL-based photodetector (VCSEL-PD)

Following the detailed analysis of the object for investigation carried out in Section 2, in this section we will conduct a comparative study of the typical characteristics of an inherent pin-photodetector and a photodetector based on a LW-VCSEL in two modes of its operation: in free-running mode and in OIL mode.

3.1 Reverse-biased free-running mode

Figure 12 depicts a common testbed for measuring static and dynamic characteristics of the VCSEL-PD using typical in photodetector's characterizing techniques and procedures [1, 3]. The testbed, besides the VCSEL-PD under test, contains a set of accessories such as optical circulator (Opneti, CIR-3-1550), master laser (PurePhotonics PPCL300, 1530–1565-nm wavelength range, 6–13.5-dBm power range), optical amplifier (Ericsson PGE 60830, 1540–1560-wavelength range, up to 20-dB gain, 13-dBm maximum output power), optical modulator (ThorLabs LN05S-FG, 1525–1605-nm wavelength range, 5-dB insertion loss, 35-GHz bandwidth), bias-T (Pasternack, PE1BT-1002, 40-GHz bandwidth) as well as corresponding DC power suppliers, digital multi-meter (INSTEK GDM-8245), and measuring tools including the same apparatuses as in **Figure 4**.

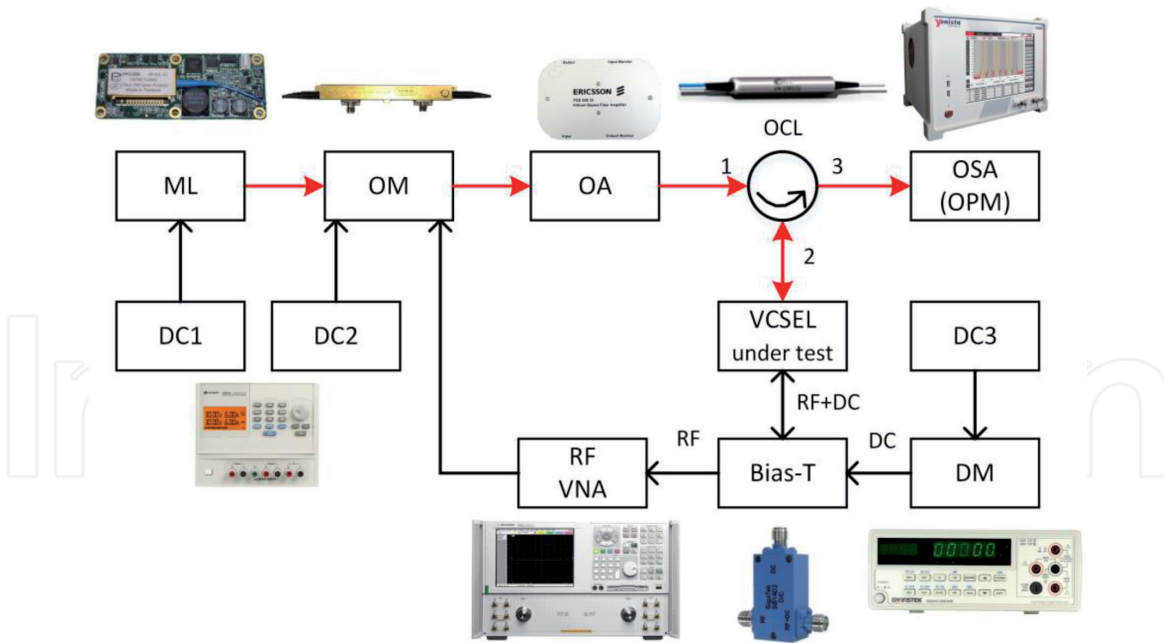


Figure 12. Common testbed for measuring static and dynamic characteristics of the VCSEL-PD under test, where ML, OM, OA, OCL, DC, DM, OSA, OPM, and RF VNA stand for master laser, optical modulator, optical amplifier, optical circulator, DC source, digital multi-meter, optical spectrum analyzer, optical power meter, and RF vector network analyzer, respectively. (optical connections are painted in red, electrical connections – in black).

Figures below demonstrate the results of measuring the key static and dynamic characteristics of the free-running VCSEL-PD using reverse DC bias from DC3. First, **Figure 13** presents dark current vs. reverse voltage characteristic. For the device under test, dark current value is not more than 70 nA at a reverse voltage up to 3 V.

Figure 14 presents the effect of reverse bias voltage on photocurrent of the VCSEL-PD under test at the 1560.95-nm incident optical powers of 1, 2, and 3 mW.

Figure 15 characterizes photocurrent vs. incident optical power of 1560.95-nm wavelength for the VCSEL-PD under test at reverse voltage of 1 V. As one can see from the Figure, the current responsivity at the initial segment of the characteristic is about 0.2 A/W, and the threshold of its linearity at a level of -1 dB is approximately 2.6 mW.

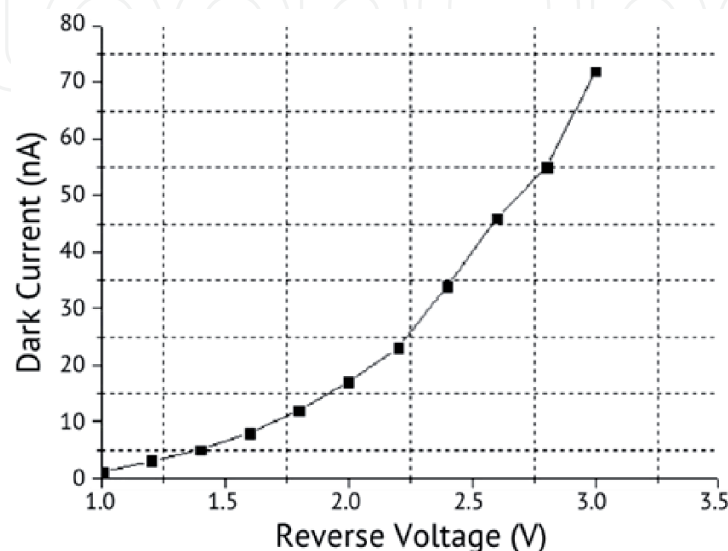


Figure 13. Dark current vs. reverse voltage characteristic.

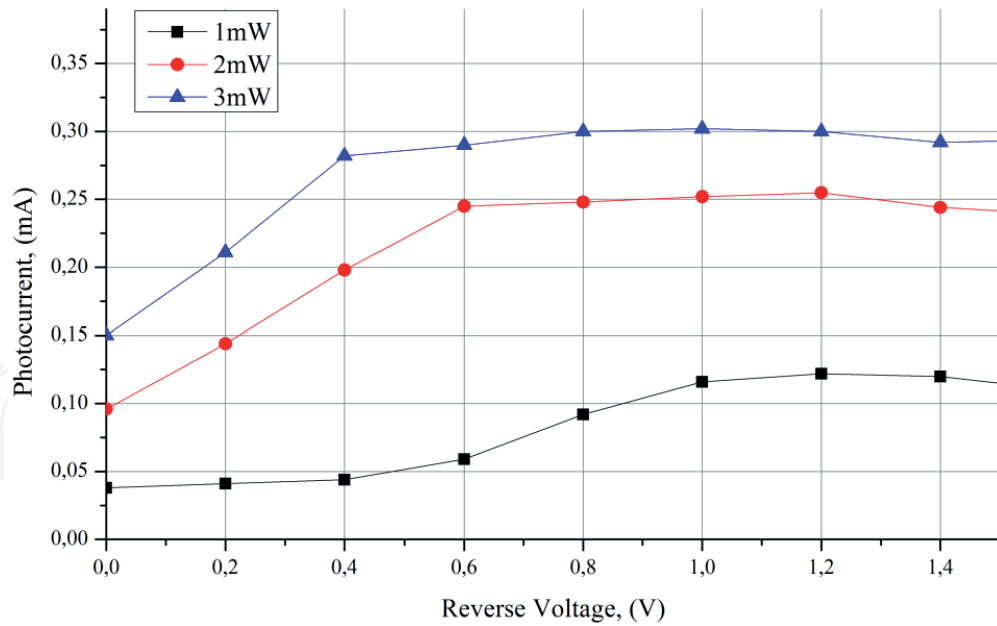


Figure 14. Photocurrent vs. reverse voltage and incident optical powers for the free-running VCSEL-PD under test.

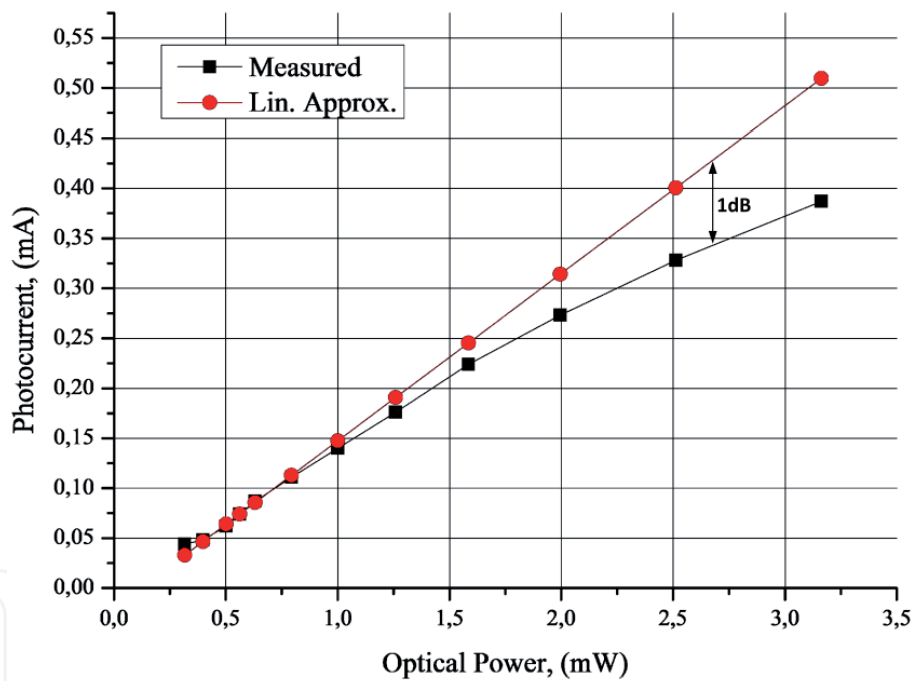


Figure 15. Photocurrent vs. incident optical power of the VCSEL-PD under test.

Figure 16 demonstrates a fine optical spectral characteristic for the VCSEL-PD under test at reverse voltage of 1 V. As one can see, due to the built-in optical cavity, the characteristic has clear resonance properties with a full bandwidth at half level of about 70 GHz.

Finally, **Figure 17** demonstrates small-signal frequency characteristic of the free-running VCSEL-PD under test at the modulating RF power of -5 dBm and the reverse voltage of 1 V. As one can see from the Figure, the total gain for EOC + OEC at the modulating frequency of 1 GHz is -38 dB at the optical power of 1 mW (brown curve 1), -28 dB at the power of 2 mW (pink curve 2), and -23.5 dB at the power of 3 mW (blue curve 3). Moreover, for all the powers, -3 -dB bandwidth is near 3.5 GHz and -5 -dB bandwidth is near 5 GHz.

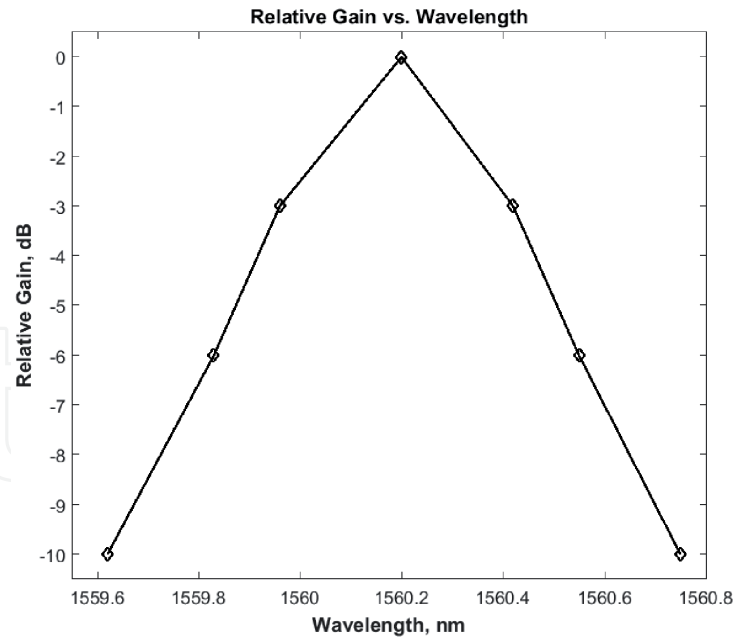


Figure 16.
 Resonance features of the VCSEL-PD under test.

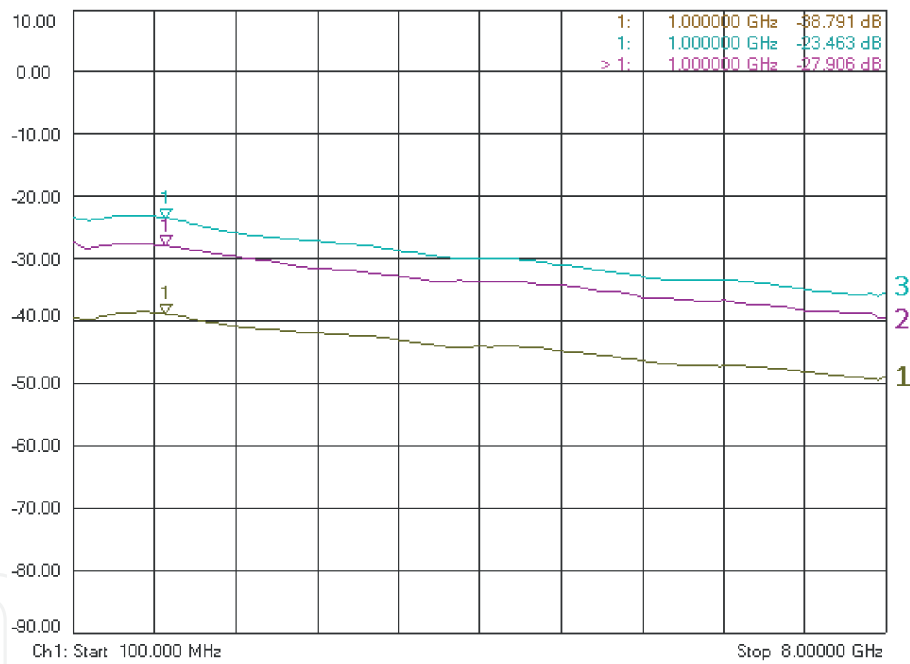


Figure 17.
 Small-signal RF characteristic of the free-running VCSEL-PD under test.

The following outcomes can be drawn from this sub-section.

- The results of measuring the dark current (**Figure 13**) showed their comparability with the specifications of the inherent pin-photodetector of model BPDV2150 (5–200 nA) used in the further study.
- The study of the photocurrent vs. reverse voltage and optical powers (**Figure 14**) made it possible to determine their significant influence. In this case, the photocurrent value increases with the optical power, which corresponds to theory and practice for inherent InP-based pin-photodiodes [24]. Also, the minimum value of an operating reverse voltage is 1 V, which was taken into account in the course of further research.

- The results of measuring the dependence of the photocurrent on the incident power (**Figure 15**) showed that the current responsivity of the VCSEL-PD under test is approximately 3 times less than that of existing pin-photodetectors operating in the microwave band. However, the VCSEL-PD has a comparable level of linearity.
- An important distinction of the VCSEL-PD is the resonance properties (**Figure 16**) arising from the presence of a built-in optical cavity, which must be taken into account in further measurements.
- Measurement of the low-signal frequency response of the VCSEL-PD under study (**Figure 17**) confirms the effect of incident optical power on RF gain as predicted in **Figure 14**, which corresponds to inherent InP pin-photodiodes [24].

3.2 Forward-biased optically injection locked mode

In this sub-section, based on the results of the Section 2 associated with the improving single-frequency regime and broadening the modulation bandwidth under OIL, as well as on the work of other authors [18–21], we will investigate the static and dynamic characteristics of the OIL-VCSEL-PD as a separate device. The measurements will be carry out using the testbed of **Figure 12** by replacing the block “VCSEL-PD under test” with the block-diagram shown in **Figure 9**.

Figure 18 addresses a photocurrent offset of the OIL-VCSEL-PD under test vs. incident OIL power at the free-running injection currents of 4, 5, and 6 mA, which according to voltage–current characteristic of **Figure 5(b)** corresponds to the forward DC voltages of 1.35, 1.5, and 1.67 V, respectively. As one can see from the Figure, the values of photocurrent offset depend on both the DC bias voltage that is in analogy with VCSEL-PD (see **Figure 14**) as well as on the incident optical power. In the result, the average photocurrent responsivity is varied from 0.03 A/W at +1.67 V to 0.04 A/W at +1.5 V.

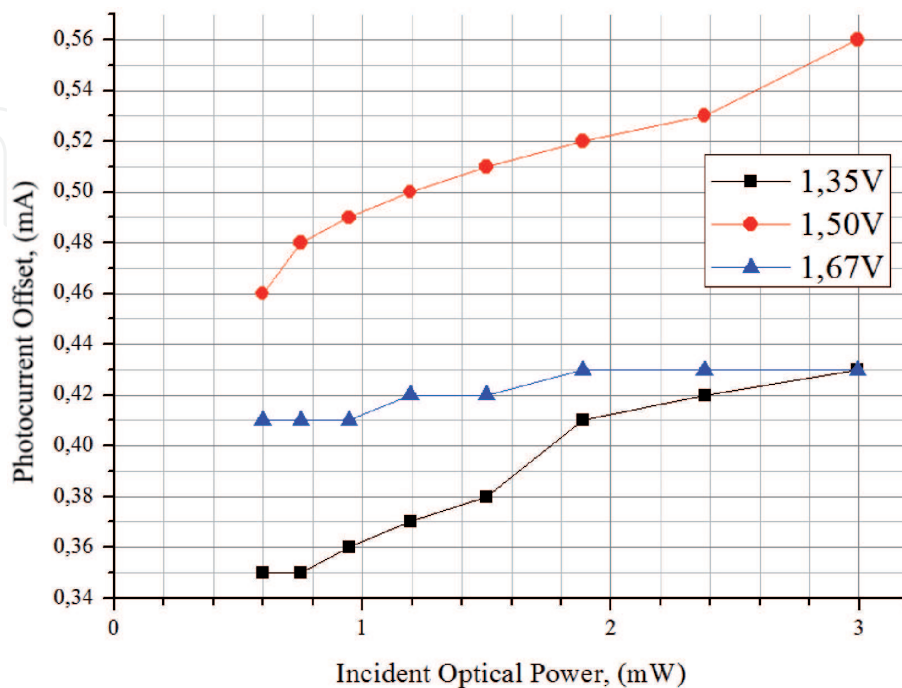


Figure 18. Photocurrent offset of the OIL-VCSEL-PD under test vs. incident OIL power.

Figure 19 presents photocurrent offset of the OIL-VCSEL-PD under test vs. detuning between the wavelengths of VCSEL-PD in OIL mode and VCSEL in free-running mode (see **Figures 6** and **10**) at incident OIL power of 2 mW and forward bias voltage of 1.5 V. A sharp drop at the detuning near +0.55 nm means that the synchronization is lost. On the other hand, a sharp peak at the offset near -0.55 nm means that the synchronization is lost. On the other hand, a sharp peak at the offset near -0.55 nm means a hop of locking from VCSEL's fundamental mode to the side mode (see **Figure 6**).

Finally, **Figure 20** presents small-signal frequency characteristic of the OIL-VCSEL-PD under test (brown curve 1) at the incident OIL power of 2 mW and detuning of +0.3 nm. Here, for comparison, a similar characteristic for an inherent pin-photodetector is shown (blue curve 2), as well as the response in the absence of an OIL signal (green curve 3).

The following outcomes can be drawn from this sub-section.

- Studying the current responsivity of the OIL-VCSEL-PD vs. the forward DC bias voltage (**Figure 18**) showed that it reaches a maximum of 0.04 A/W at a voltage of 1.5 V, which is 5 times lower compared to the free-running VCSEL-PD (see **Figure 15**).
- Studying the current responsivity of the OIL-VCSEL-PD vs. the detuning between the wavelengths of VCSEL-PD in OIL mode and VCSEL in free-running mode (**Figure 19**) showed that the locking range inside the fundamental mode is near 1.1 nm and the average slope of current responsivity is 0.7 mA/nm, which must be taken into account in further studies.
- Studying the small-signal frequency characteristic of the OIL-VCSEL-PD (**Figure 20**) showed that locking emission of the master laser leads to an approximately 30 dB increase in the gain, but its bandwidth is significantly lower compared to the similar characteristic of **Figure 11**. The reason for this effect is the high loss (7.2 dB) in the optical probe (see Section 2), which must be taken into account in the course of further studies.

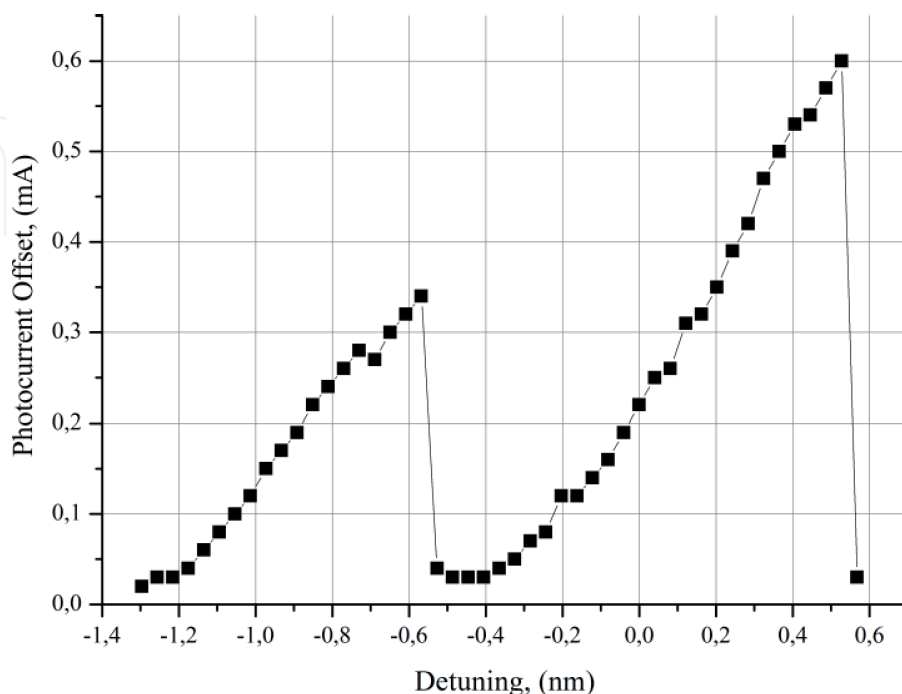


Figure 19.
Photocurrent offset of the OIL-VCSEL-PD under test vs. detuning.

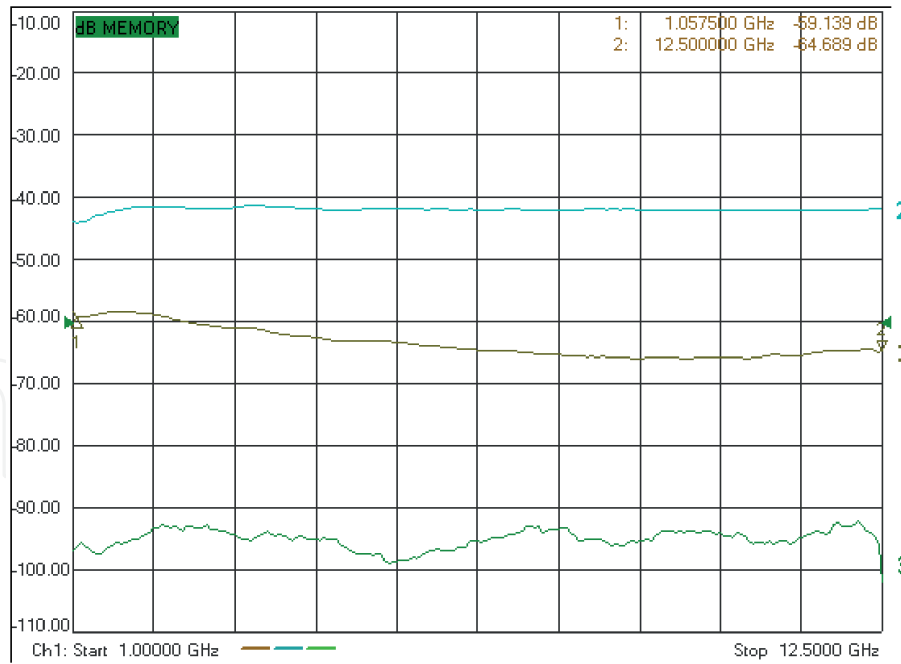


Figure 20.
Small-signal frequency characteristic of the OIL-VCSEL-PD under test.

4. Comparative experimental research using a typical MWP circuit

The previous section was referred to a comparative analysis of the VCSEL-based photodetector properties as a separate device in two modes of its operation, such as free running and optically injection locking. Continuing and expanding the study, in this section, it is considered as an element of a typical MWP circuit including, as described in the Introduction, three cascaded parts: EOC, optical processing unit (OPU), and OEC. Moreover, in this case, for completeness of coverage, three research objects are considered: a pin-photodiode, free-running VCSEL-PD, and OIL-VCSEL-PD. The general testbed for conducting experimental research is presented in **Figure 21**.

In the Figure, the EOC unit contains the tunable semiconductor laser (PurePhotonics PPCL300, 1535–1565-nm wavelength range, 6–13.5-dBm power

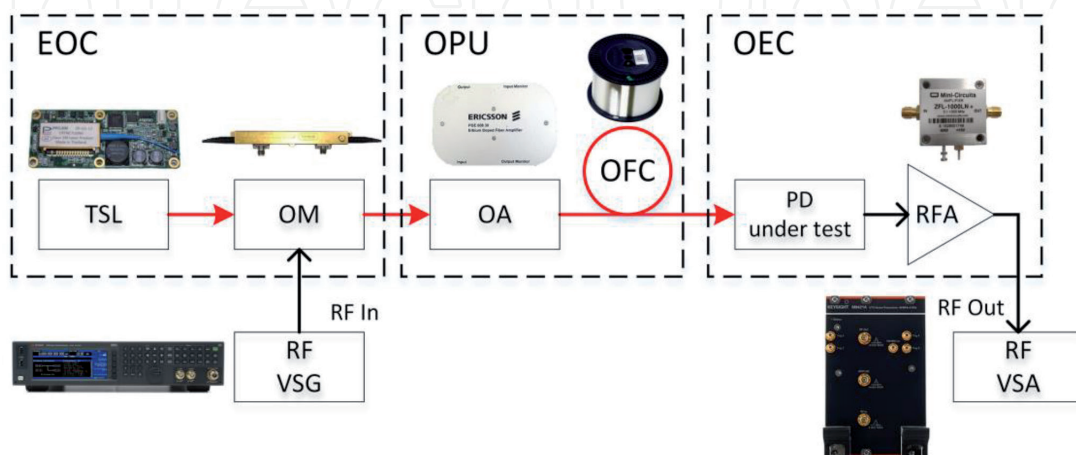


Figure 21.
General testbed for conducting experimental research, where TSL, OM, OA, OFC, PD, RFA, RF VSG and RF VSA stand for tunable semiconductor laser, optical modulator, optical amplifier, optical fiber coil, photodetector, RF amplifier, RF vector signal generator, and RF vector signal analyzer, respectively. (optical connections are painted in red, electrical connections – in black).

range) and the optical modulator (ThorLabs LN05S-FG, 1525–1605-nm wavelength range, 5-dB insertion loss, 35-GHz bandwidth). In addition, the OPU consists of optical amplifier (Ericsson PGE 60830, 1540–1560-wavelength range, up to 20-dB gain, 13-dBm maximum output power) and optical fiber coil (SMF-28+, 5 km). Finally, OEC unit includes PD under test (Finisar, BPDV2150, 43-GHz bandwidth, 0.6-A/W responsivity, or VCSEL-PD, or OIL-VCSEL-PD) and home-made RF amplifier (1–6-GHz operation range, 30-dB gain, 2.2-dB noise figure). Note that in all experiments, the same EOC is used with a TSL different in emitted power and wavelength, respectively. Besides, in connection with the above-mentioned structural features of the photodetectors under test, for the pin-PD a direct connection to the circuit was used, as in **Figure 21**, while VCSEL-based devices were connected to the circuit through an optical circulator (see **Figure 12**).

To provide a practical focus, in the way of the experiments such an important quality indicator for a FOCS and wireless RES as an error vector magnitude (EVM), which in the first approximation is inversely proportional to the square root of the signal-to-noise ratio [25], is evaluated. To implement this measurement, using the VSG (Keysight N8152B), a digital signal at a bitrate of 120 Mbps with 16-position quadrature amplitude modulation (16-QAM) on a RF carrier in the 1–6 GHz band, is applied to the RF input of the OM and the output signal of the RFA is recorded using the VSA (Keysight M9421A).

Figure 22 presents the results of the comparative experiments using the optimal operating regimes that conclude from the Section 3. In the same graph, the horizontal dashed line marks the standard limit for transmitting 16-QAM signals in the emerging 5th generation cellular telecommunications network [26]. For the best vision, there are two insets in the Figure showing constellation diagrams in specific points.

The following outcomes can be drawn from this Figure.

- When using any of three variants of the photodetector under study, the EVM levels, which determines the quality of signal processing in the MWP circuit, turned out to be significantly lower than the threshold value.
- The smallest values of this parameter, i.e. the best processing quality, and independence from the frequency of the RF carrier are obtained when using pin-photodiode, which is determined by its above mentioned bandwidth up to 43 GHz.

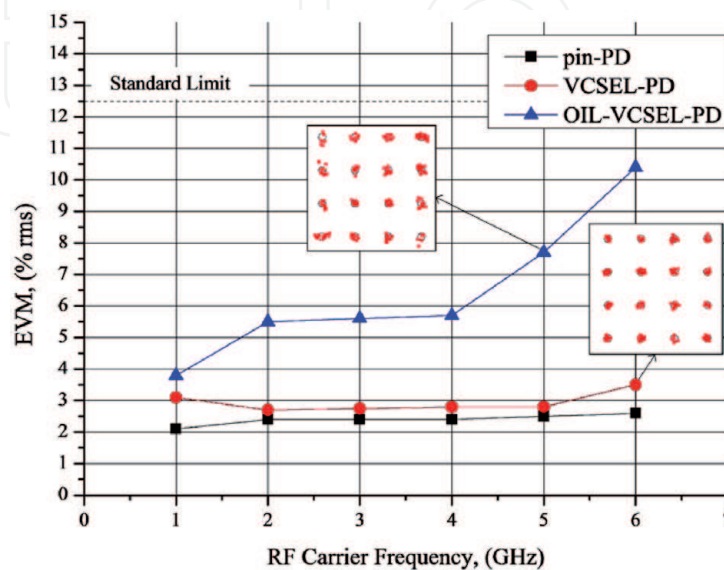


Figure 22. Study of signal quality for a typical microwave-photonics circuit when processing high-speed data with multi-position quadrature amplitude modulation.

- Slightly large values of the EVM are observed, when using a free-running VCSEL-based photodetector. The increase in the EVM at the upper RF carrier frequency noted in the graph is most likely due to its limited bandwidth (see **Figure 17**).
- The largest values of the EVM that increase with the RF carrier are obtained when using an OIL-VCSEL-PD, which is associated with its poorest photo-current responsivity, increased noise due to operating in the laser mode and limited bandwidth (see **Figure 20**) due to the above-mentioned losses in the optical probe.

5. Conclusion

In this Chapter, a detailed comparative experimental study was carry out to pursue advanced performances corresponding to the key parameters of two VCSEL-based photodetectors operating in free-running or optically injection locked mode as well as an inherent pin-photodetector. During the preliminary study, the key static and dynamic parameters were quantitatively determined and the optimal operating modes were derived for both versions of VCSEL-based photodetector as a separate microwave-photonics circuit element. Based on them, a final study was carried out to evaluate the processing quality when the both versions of VCSEL-based photodetectors or an inherent pin-photodetector work as an optical-to-electrical converter of a typical microwave circuit, which can become the core when developing a cost- and power-efficient base station for a mobile cellular telecommunication system of fifth generation [27], as well as for an advanced Wi-Fi system [28] of fiber-wireless architecture, which will significantly increase its service area. As a result, it was confirmed that better processing quality can be obtained by using the free-running VCSEL-based photodetector version.

Further research will focus at a detailed comparative studying the features of the VCSEL-based photodetectors, at expanding their bandwidth to the millimeter wavelength range, as well as at the development of optimal microwave-photonics circuits using one of these devices as an optical-to-electrical converter.

Acknowledgements

The authors thank Dr. V. P. Yakovlev for the provided laser samples and JSC “Akmetron”, Moscow, Russian Federation for the provided measuring instruments.

Conflict of interest

The authors declare the lack of the ‘conflict of interest’.

IntechOpen

Author details

Mikhail E. Belkin^{1*}, Leonid I. Zhukov¹, Dmitriy A. Fofanov¹, Mikhail G. Vasil'ev²
and Alexander S. Sigov¹

1 MIREA - Russian Technological University, Moscow, Russian Federation

2 Kurnakov Institute of General and Inorganic Chemistry, Russian Academy of Sciences, Moscow, Russian Federation

*Address all correspondence to: belkin@mirea.ru

IntechOpen

© 2021 The Author(s). Licensee IntechOpen. This chapter is distributed under the terms of the Creative Commons Attribution License (<http://creativecommons.org/licenses/by/3.0>), which permits unrestricted use, distribution, and reproduction in any medium, provided the original work is properly cited. 

References

- [1] Gower J. Optical Communication Systems. Second Edition. Prentice Hall, 1993, 696 pp.
- [2] Urick, V. J., McKinney, J. D., Williams, K. J. (2015) Fundamentals of Microwave Photonics, Hoboken, New Jersey.
- [3] Belkin M. E. "Multiscale Computer Aided Design of Microwave-Band P-I-N Photodetectors," In book "Photodetectors" Ed. By S. Gateva – InTech Open, Chapter 6, pp. 231-250, 2012. <https://www.intechopen.com/books/photodetectors/multiscale-computer-aided-design-of-microwave-band-p-i-n-photodetectors>
- [4] M.E. Belkin, V. Golovin, Y. Tyschuk, M. Vasil'ev, and A.S. Sigov, "Computer-Aided Design of Microwave-Photonics-based RF Circuits and Systems," In book "RF Systems, Circuits and Components" Ed. by M. Reaz and M. Bhuiyan – InTech Open, Chapter 4, pp. 61-81, 2018. <https://www.intechopen.com/books/rf-systems-circuits-and-components/computer-aided-design-of-microwave-photonics-based-rf-circuits-and-systems>
- [5] VCSELS: Fundamentals, Technology and Applications of Vertical-Cavity Surface-Emitting Lasers. Ed. R. Michalzik. Springer Series in Optical Sciences 166; 2013. ISBN 978-3-642-24986-0
- [6] Koyama A. F. Recent advances of VCSEL photonics. IEEE Journal of Lightwave Technology 2006. 24(12) 4502-4513
- [7] Kapon E., Sirbu A. Long-wavelength VCSELS: Power-efficient answer. Nature Photonics 2009; 3, 27-29 doi:10.1038/nphoton.2008.266.
- [8] Belkin M.E., Belkin L., Loparev A., Sigov A.S., Iakovlev V. Long Wavelength VCSELS and VCSEL-Based Processing of Microwave Signals // In book "Optoelectronics – Advanced Materials and Devices", Ed. by S. Pyshkin and J. Ballato, – InTechOpen, Croatia, 2015, Chapter 6, pp. 231-250. <https://www.intechopen.com/books/optoelectronics-materials-and-devices/long-wavelength-vcsels-and-vcSEL-based-processing-of-microwave-signals>
- [9] K. Kishino, M. Unlu, J. Chyi, L. Arsenault, and H. Morkoc, "Resonant-cavity enhanced (RCE) photodetectors," IEEE Journal on Quantum Electronics, vol. 27, pp. 2025-2034, 1991.
- [10] X. Duan, Y. Huang, X. Ren, et al., "Long Wavelength Multiple Resonant Cavities RCE Photodetectors on GaAs Substrates," IEEE Transactions on Electron Devices, Vol. 58, No. 11, p. 3948-3953, Nov. 2011.
- [11] J. Guo, Y. Zuo, Y. Zhang, et al., "Simulation Research of Nonlinear Behavior Induced by the Charge-Carrier Effect in Resonant-Cavity-Enhanced Photodetectors," IEEE Journal of Lightwave Technology, vol. 25, No 9, p. 2783-2790, Sept. 2007.
- [12] M. Casalino, L. Sirleto, L. Moretti, et al., "Fabrication and Characterization of Resonant Cavity Enhanced Silicon Photodetectors at 1.55 μm ," 5th International Conference of Group IV Photonics, 2008, p. 1-3.
- [13] Qi Wei, Kai Liu, Yo. Huang, et al., "A pair of integrated optoelectronic chips for optical interconnects," Asia Communications and Photonics Conference (ACP), 2018, 2 pp.
- [14] T. Knodl, et al., "RCE Photodetectors based on VCSEL Structures," IEEE Photonics Technology Letters, vol. 11, no. 10, p. 1289-1291, 1999.

- [15] Belkin M. E. Investigation of the static and dynamic characteristics for a wafer-fused C-band VCSEL in the mode of the optical-electric converter, *Technical Physics Letters*, 2018, Vol. 44, No. 1, pp. 32-35. DOI: 10.1134/S1063785018010030 © Pleiades Publishing, Ltd., 2018. ISSN 1063-7850
- [16] M. E. Belkin, V. Golovin, Y. Tyschuk, and A.S. Sigov. Model of an active optoelectronic switchable element for integrated photonics-based optical beamforming network. 2017 Progress In Electromagnetics Research Symposium - Spring (PIERS), 2017, pp. 1592-1593. <https://ieeexplore.ieee.org/document/8262002> (DOI: 10.1109/PIERS.2017.8262002)
- [17] Belkin M. E., Alyoshin A., and Fofanov D., "Microwave Photonics Characterization and Application of Long-Wavelength VCSELs in Atypical Regimes," 2-nd International Conference on Photonics Research, InterPhotonics-2019, Antalya, Turkey.
- [18] Q. Gu, W. Hofmann, M.-C. Amann, L. Chrostovski, "Optically Injection-Locked VCSEL for Bi-directional Optical Communication," 2008 Conference on Lasers and Electro-Optics (CLEO2008), p. 1-2.
- [19] Q. Gu, W. Hofmann, M.-C. Amann, L. Chrostovski, "Optically Injection-Locked VCSEL of a Duplex Transmitter/Receiver," *IEEE Photonics Technology Letters*, vol. 20, no. 7, p. 463-465, 2008.
- [20] Erwin K. Lau, Liang Jie Wong, Ming C. Wu, "Enhanced Modulation Characteristics of Optical Injection-Locked Lasers: A Tutorial," *IEEE Journal of Selected Topics in Quantum Electronics*, v. 15, no. 3, p. 618-633, 2009.
- [21] L. Chrostowski, X. Zhao, and C. J. Chang-Hasnain, "Microwave Performance of Optically Injection-Locked VCSELs," *IEEE Transactions on Microwave Theory and Techniques*, v. 54, no. 2, p. 788-796, 2006
- [22] Fang A.W., Koch B., Norberg, E., et al. Heterogeneous integration as a manufacturing platform for photonic integrated circuits. // *IEEE Photonics Conference (IPC)*, 2013. – P. 87-88.
- [23] Belkin, M.E., Iakovlev, V., Wafer fused long-wavelength VCSELs for analog photonics applications, *Conference Digest - IEEE International Semiconductor Laser Conference ISLC2016*, Kobe, Japan, 2016. art. no. 7765770. <https://ieeexplore.ieee.org/document/7765770>
- [24] *Handbook of Optical Components and Engineering*. – Ed. by K. Chang, John Wiley & Sons, Hoboken, New Jersey, 2003, 1380 pp.
- [25] R. A. Shafik, Md. S. Rahman, AHM R. Islam, "On the Extended Relationships Among EVM, BER and SNR as Performance Metrics," *Proceeding of 4th International Conference on Electrical and Computer Engineering, ICECE 2006*, 19-21 December 2006, Dhaka, Bangladesh, p. 408-411.
- [26] ETSI, "Minimum requirements for Error Vector Magnitude," in *TECHNICAL SPECIFICATION, LTE; Evolved Universal Terrestrial Radio Access (E-UTRA); User Equipment (UE) radio transmission and reception (3GPP TS 36.101 version 14.3.0 Release 14)*, ETSI, 2017-04, p. 215.
- [27] M. E. Belkin, T. Bakhvalova, and A.C. Sigov, "Design Principles of 5G NR RoF-Based Fiber-Wireless Access Network"; In book "Recent Trends in Communication Networks", IntechOpen, London, UK, p. 121-145, 2020. DOI: 10.5772/intechopen.90074. Available online: <https://www.intechopen.com/online-first/design-principles-of-5g-nr-rof-based-fiber-wireless-access-network>

[28] 8802-11-2012 - ISO/IEC/IEEE
International Standard - Information
technology--Telecommunications and
information exchange between systems
Local and metropolitan area networks--
-Specific requirements Part 11:
Wireless LAN Medium Access Control
(MAC) and Physical Layer (PHY)
Specifications.

IntechOpen

IntechOpen